

Supplementary Information

For

Preparing Nitrogen and Sulfur Codoped Carbon Quantum Dots to Achieve Labeling of Bovine Serum Albumin

Wanqing Li ¹, Xue Chen ¹, Xipeng Dong ¹, Zizhuo Zhai ¹, Yu Kang ², Pudun Zhang^{1,2,*}

1. College of Chemistry, Beijing University of Chemical Technology, Beijing 100029,
China

2. Analysis and Test Center, Beijing University of Chemical Technology, Beijing
100029, China

* Corresponding author:

Pudun Zhang

No. 15 Beisanhuan East Road, Chaoyang, Beijing 100029, China.

Tel & Fax: +86 010 64417634;

E-mail address: zhangpd@mail.buct.edu.cn

1. Separation of N,S-CQDs by silica column chromatography

A certain amount of silica with 100-120 mesh was first activated at 110 °C for 2 hours and then ultrasonically dispersed in petroleum ether (A.R.). The homogenized silica suspension was filled into a glass column (30 cm in length × 1 cm in internal diameter) via a separatory funnel. Keep tapping the glass column with a plastic stick continuously and gently to ensure that the filling is uniform and compact during this process. Bubbles are not allowed to form in the column.

Before separation, 20 mg of crude N,S-CQDs was carefully added into the silica column, avoiding the spreading of sample. The analytical grade solvents, including acetone, ethanol, methanol, and pure water with 20-30 mL were sequentially added into the column to separate the CQDs, and a UV light (365 nm) was applied to irradiate the column. Three well-separated color bands were seen and collected separately using a series of prenumbered weighing bottles. Every bottle was evaporated and weighed to quantify the collected component. At last, the chromatogram was plotted based on the weight of each bottle (Figure S1a). It clearly shows that the crude N,S-CQDs consist of blue, yellow and red CQDs (B-CQDs, Y-CQDs, R-CQDs) with a ratio of about 1:1:1 (Figure S1b).

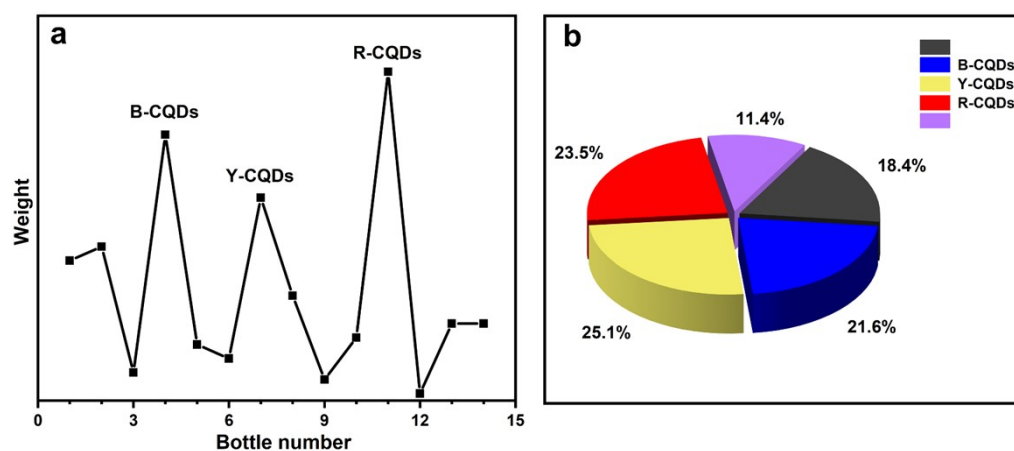


Figure S1. Column chromatogram of crude N,S-CQDs. (a) Three components emitted blue, yellow and red fluorescence are collected, which are named after B-CQDs, Y-CQDs and R-CQDs, respectively. (b) The mass distribution of each component after column chromatographic separation.

2. Spectral characterizations of crude N,S-CQDs

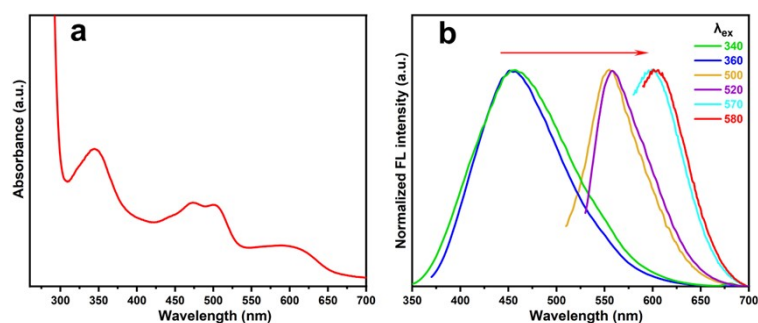


Figure S2. (a) The UV-vis spectrum and (b) the normalized fluorescence spectra of crude CQDs.

3. The fluorescence spectra of three separated components under varied excitation wavelengths.

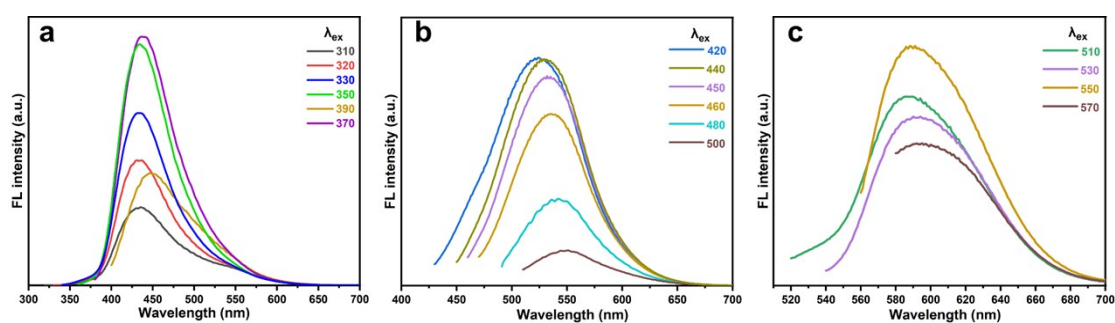


Figure S3. Fluorescence spectra of (a) B-CQDs, (b) Y-CQDs and (c) R-CQDs under varied excitation wavelengths.

4. Investigation of the fluorescence stability of the three N,S-CQDs

The fluorescence stability of the three N,S-CQDs was investigated by their tolerance to pH and salt solution as well as the preservation and continuously long-time irradiation. As shown in Figure S4a, both B-CQDs and Y-CQDs display excellent fluorescence stability in the pH range 1-13, while R-CQDs show an excellent fluorescence stability in the pH range 1-11. When pH is increased to higher than 12, the fluorescence intensity of R-CQDs increases greatly, possibly due to the deprotonation. In addition, the fluorescence intensities of the three N,S-CQDs also display super stability in high-concentration salt solutions (Figure S4b), in 180 days (Figure S4c), as well as continuously irradiating 9000 s (Figure S4d). The results indicate that the three CQDs exhibit outstanding photostability, anti-bleaching and robust environmental resilience.

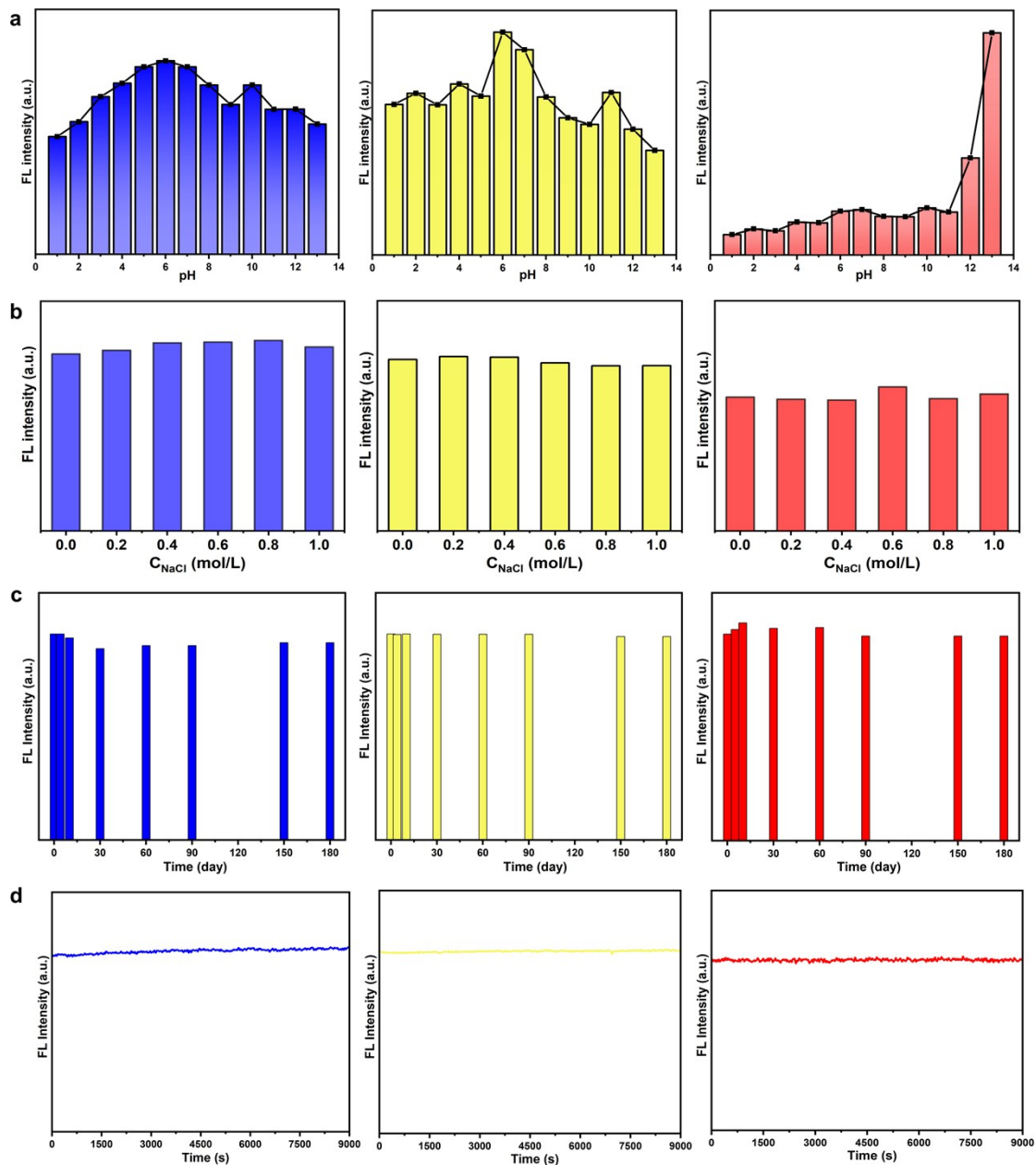


Figure S4. Assessment of the fluorescence stability of the three N,S-CQDs by (a) changing the pH of each solution in the range 1-13, (b) adding varied concentrations of NaCl (0-1.0 mol L⁻¹), (c) standing for 180 days, as well as (d) continuously irradiating 9000 s.

5. UV-vis spectrum of R-CQDs in the range 230-850 nm

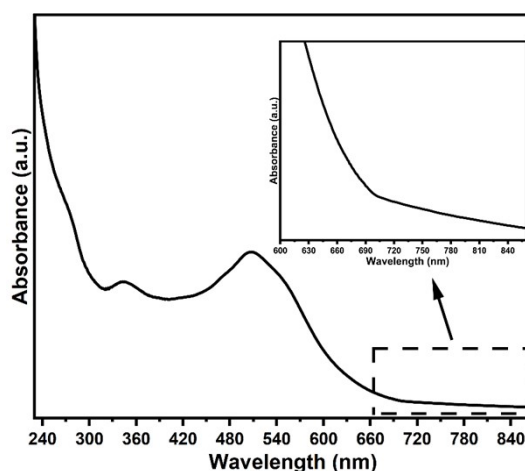


Figure S5. UV-vis spectrum of R-CQDs. The inset shows an obvious rise in the absorption range 600-850 nm. An extinction coefficient of $1.29 \text{ L g}^{-1} \text{ cm}^{-1}$ at 808 nm was achieved.

6. Photothermal performance of R-CQDs

The photothermal performance of R-CQDs was investigated using a method similar to our previous work^[1] except that the 808 nm laser was used to replace the 650 nm laser. By changing the power of laser (Figure S6a), a series of photothermal curves of 1.0 mg mL^{-1} R-CQDs solution can be collected. It shows that the temperature elevation (ΔT) increases with the power of 808 nm laser. When the power is 1.25 W cm^{-2} , the ΔT of $23.7 \text{ }^\circ\text{C}$ is achieved after 10 min. Furtherly, under irradiation by 1.0 W cm^{-2} laser, the ΔT of R-CQDs solution increases with the concentration of R-CQDs (Figure S6b), and the maximum ΔT of $25.2 \text{ }^\circ\text{C}$ is achieved when the concentration is 5.0 mg mL^{-1} . The multiple on/off cycles of R-CQDs solution (5.0 mg mL^{-1}) under irradiation of 808 nm laser (Figure S6c) demonstrate the excellent photothermal stability of CQDs. The photothermal conversion efficiency (PCE) can be drawn from the plot of cooling time versus $-\ln\theta$ (Figure S6d) after irradiating by 808 nm laser (1.0 W cm^{-2}). The detailed calculation procedure was described in the Supporting Information of our previous work.^[1]

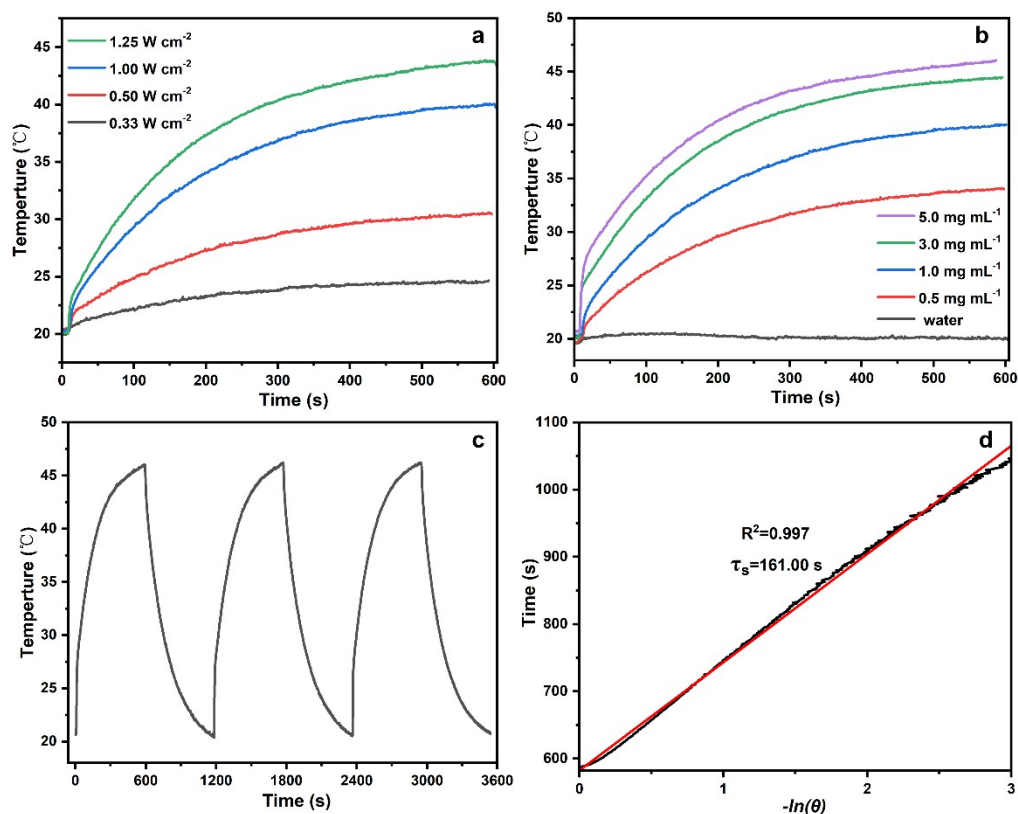


Figure S6. Photothermal performance of R-CQDs. (a) Temperature variation of 1.0 mg mL⁻¹ R-CQDs aqueous solution during 10 min of irradiation with different power lasers, (b) Temperature change of pure water and aqueous solution of R-CQDs at different concentrations during 808 nm laser irradiation (1.0 W cm⁻², 10 min), (c) On/off cycle of 5.0 mg mL⁻¹ R-CQDs solution under three laser irradiations and (d) plot of cooling time versus $-\ln\theta$ (the negative natural logarithm of the temperature driving force obtained from the cooling state).

7. Characterization of three N,S-CQDs by XRD

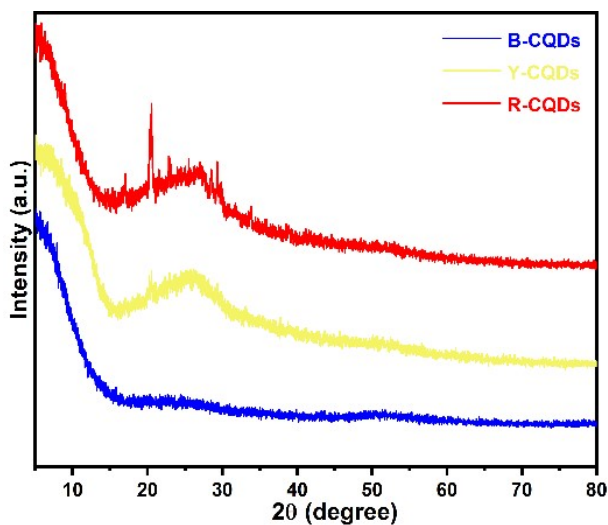


Figure S7. The XRD patterns of B-CQDs, Y-CQDs and R-CQDs.

8. Elemental analysis results of three N,S-CQDs

Table S1. Elemental analysis results of the CQDs.

| Type | C% | H% | N% | S% |
|--------|-------|------|-------|------|
| B-CQDs | 40.22 | 4.17 | 13.54 | 2.65 |
| Y-CQDs | 45.16 | 3.84 | 15.69 | 5.64 |
| R-CQDs | 40.43 | 3.97 | 15.68 | 7.38 |

The elemental analysis result shows that the amounts of sulfur (S) gradually increase from B-CQDs to Y-CQDs and further to R-CQDs, while the amounts of nitrogen (N) are nearly unchangeable. Although the S/N mass ratio of B-CQDs, Y-CQDs and R-CQDs increases from 0.20 to 0.36 and further to 0.47, the band intensities of thiocyanate/isothiocyanate groups in the FTIR spectra (Figure 2 in main text) do not increase, and even the one of isothiocyanate functional groups of R-CQDs decreases significantly. This indicates that considerable amounts of S are converted into other S-containing functional groups. Correspondingly, the high-resolution S 2p XPS spectra (Figure 3e in main text) confirm the presence of thiophene or thiazole. The increase of thiophene and thiazole in CQDs expands the conjugated sp^2 structure, and reduce the HOMO-LUMO band gap of CQDs, which contributes to the redshift of the emission wavelength. Moreover, the increase in the S/N ratio also facilitates the formation of the $-N=C=S$ functional group, which provides a possibility to directly label protein by the obtained N,S-CQDs.

9. High-resolution S2p spectrum of the XPS results of Fluorescein isothiocyanate (FITC) and potassium thiocyanate (KSCN)

In order to distinguish isothiocyanate group ($-N=C=S$) and thiocyanate group ($-S-C\equiv N$) by using XPS, two compounds, Fluorescein isothiocyanate (FITC) and potassium thiocyanate (KSCN), were analyzed by XPS and the deconvoluted S2p spectra of the two compounds are displayed in Figure S8. It clearly shows the difference between them. By comparing the S2p spectra of FITC, KSCN and those of the three N,S-CQDs (Figure 3e in the core manuscript), a conclusion that $-N=C=S$ group exists on R-CQDs while $-S-C\equiv N$ group on both B-CQDs and Y-CQDs can be easily drawn.

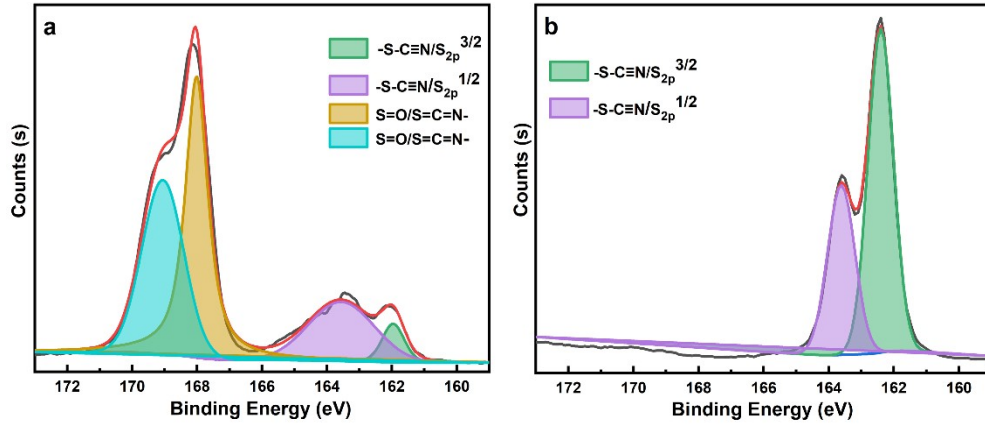
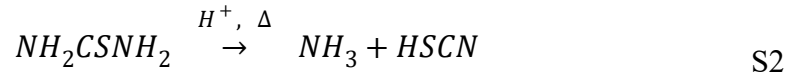
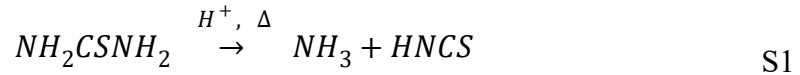


Figure S8. The high-resolution S 2p XPS spectra of (a) FITC and (b) KSCN.

10. Mechanism of isothiocyanate/thiocyanate (-N=C=S/-S-C≡N) formation on N,S-CQDs

Generally, thiourea would be dissociated into ammonia (NH₃) and thiocyanic acid/isothiocyanic acid (H-S-C≡N/H-N=C=S or HSCN/HNCS) under acidic condition (due to the presence of citric acid) at high temperature according to equations S1 and S2,

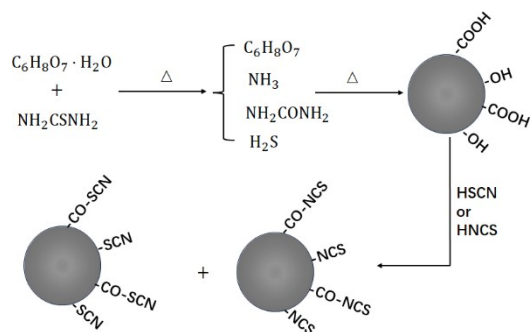


Actually, HSCN would also convert to HNCS under high temperature, and vice versa.

Besides, thiourea would also react with H₂O (come from the dissociation of citric acid monohydrate) to generate urea and hydrogen sulfide (H₂S) according to equation S3,



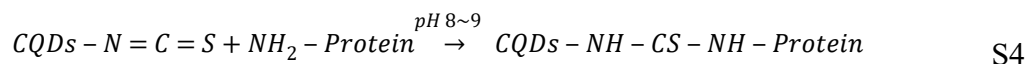
The generated NH₃, urea and H₂S would react with citric acid under solvothermal conditions to form the N,S-CQDs with surface adorned the carboxyl and hydroxyl groups, which will further react with HSCN or HNCS to form the SCN/NCS-functionalized CQDs. The schematic formation procedure is shown in Scheme S1.



Scheme S1. Schematic formation of SCN or NCS-functionalized CQDs.

11. Mechanism of the selective attachment of proteins by isothiocyanate-functionalized R-CQDs

The mechanism of the selective attachment of proteins by isothiocyanate-functionalized R-CQDs is similar to that by fluorescein isothiocyanate (FITC), which follows a nucleophilic reaction of the primary amino group of protein, in which the “C” in N=C=S group plays a role of electrophilic center. The reaction formula (S4) is as following,



At weak basic condition (pH 8-9), the ϵ -NH₂ groups of lysine residue are nucleophilic and attack the electrophilic “C” atom of isothiocyanate, forming a stable and substituted thiocarbamide bond. This reaction should be finished in carbonate buffer solution (pH 8.5).

12. Absorption spectrum of R-CQDs and fluorescence spectra of BSA

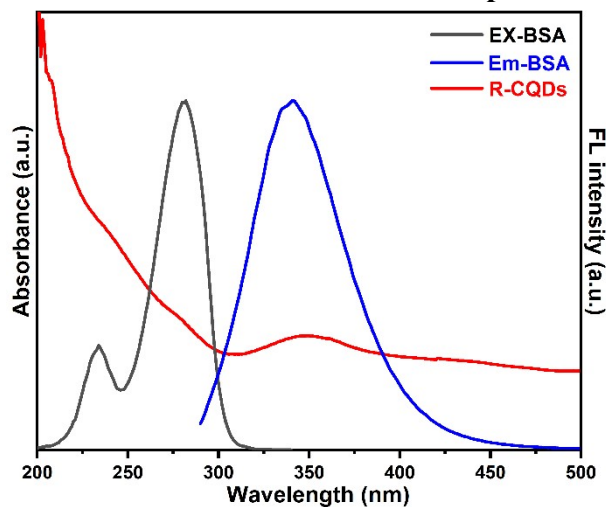


Figure S9. The UV-vis absorption spectrum of R-CQDs and the fluorescence excitation and emission spectra of BSA.

13. Hill model for describing the interaction between BSA and R-CQDs^[1-3]

The reaction between BSA and R-CQDs can be expressed by



Thus, each BSA has n binding sites for R-CQDs. R-CQDs@BSA is a BSA fully saturated by n R-CQDs. When the thermodynamic equilibrium is reached, the dissociation equilibrium coefficient, K_D , can be written by

$$K_D = \frac{c_{BSA} \cdot c_{R-CQDs}^n}{c_{R-CQDs@BSA}} \quad S6$$

where c_{R-CQDs} , c_{BSA} and $c_{R-CQDs@BSA}$ represent the concentrations of free R-CQDs, non-binding BSA and R-CQDs@BSA, respectively. Generally, an apparent dissociation coefficient K_D' , defined as the concentration at which half of the BSA are saturated, is often used to replace K_D ^[2]

$$K_D' = K_D^{\frac{1}{n}} \quad S7$$

Noting that K_D' is essentially a concentration.

According to equations S5-7, the ratio of the concentration of the BSA labeled by R-CQDs to the initial concentration of BSA (c_{BSA}^0) is given by

$$\frac{c_{R-CQDs@BSA}}{c_{BSA}^0} = \frac{1}{1 + \left(\frac{K_D'}{c_{R-CQDs}} \right)^n} \quad S8$$

When labeling reaction reaches equilibrium,

$$c_{R-CQDs@BSA} = c_{BSA}^0 - c_{BSA} \quad S9$$

Since BSA can emit fluorescence at 340 nm, and its intrinsic fluorescence intensity is proportional to BSA concentration, we therefore substitute the fluorescence intensity for the concentration in equation S8, and the ratio is represented by F^* ,

$$F^* = \frac{F_{BSA}^0 - F_{BSA}}{F_{BSA}^0} = \frac{1}{1 + \left(\frac{K_D'}{c_{R-CQDs}} \right)^n} \quad S10$$

where F_{BSA}^0 and F_{BSA} are the fluorescence intensity of BSA at 340 nm in the absence

and presence of R-CQDs, respectively.

By adding varied concentrations of R-CQDs into 1.0 mL of 0.1 mg mL⁻¹ BSA solutions, a series of fluorescence spectra were collected under excitation at 280 nm (Figure 4b in core manuscript). Accordingly, the ratio of intensity (F^*) is plotted versus the concentration of added R-CQDs, as shown in Figure 4e in core manuscript. The apparent dissociation constant (K_D') and the Hill coefficient (h) can therefore be obtained by fitting the data using equation (6).

14. Determination of the binding equilibrium constant and the number of binding sites between BSA and R-CQDs^[4-6]

According to equation S5, a binding equilibrium constant K can be derived,

$$K = \frac{c_{\text{R-CQDs@BSA}}}{c_{\text{BSA}} \cdot c_{\text{R-CQDs}}^n} \quad \text{S11}$$

K is the reciprocal of the dissociation equilibrium coefficient K_D .

By combining equation S9, equation S11 can be transformed into equation S12,

$$\frac{c_{\text{R-CQDs@BSA}}}{c_{\text{BSA}}} = \frac{c_{\text{BSA}}^0 - c_{\text{BSA}}}{c_{\text{BSA}}} = K \cdot c_{\text{R-CQDs}}^n \quad \text{S12}$$

Furtherly, the intrinsic fluorescence intensity of BSA is often used to substitute for its concentration, and equation S12 can therefore be changed to equation S13,

$$\frac{F_{\text{BSA}}^0 - F_{\text{BSA}}}{F_{\text{BSA}}} = K \cdot c_{\text{R-CQDs}}^n \quad \text{S13}$$

Taking logarithm for both ends of equation S13, equation S14 can be obtained,

$$\lg \frac{F_{\text{BSA}}^0 - F_{\text{BSA}}}{F_{\text{BSA}}} = \lg K + n \lg c_{\text{R-CQDs}} \quad \text{S14}$$

The binding constant (K) and the number of binding sites (n) are therefore achieved by plotting the $\lg \frac{F_{\text{BSA}}^0 - F_{\text{BSA}}}{F_{\text{BSA}}}$ versus the $\lg c_{\text{R-CQDs}}$ (Figure S10) using the data of Figure 4b in core manuscript.

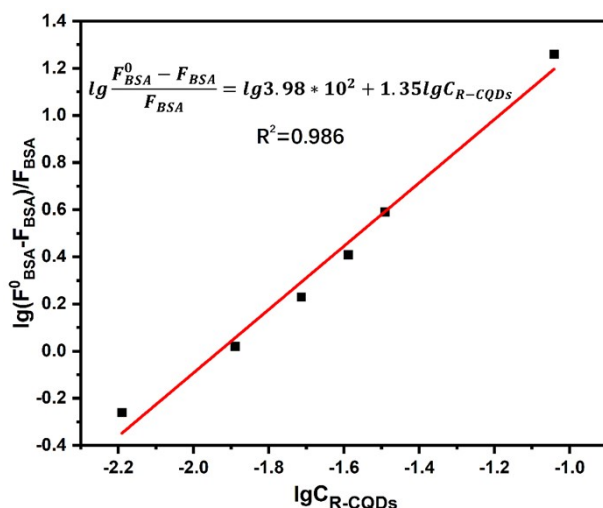


Figure S10. The linear relationship between $\lg \frac{F_{BSA}^0 - F_{BSA}}{F_{BSA}}$ and $\lg C_{R-CQDs}$.

15. Correction factor (CF) of R-CQDs

An absorption at 350 nm was used to correct the contribution of R-CQDs to the absorbance of labeled BSA at 280 nm since BSA has no absorption at 350 nm. The absorbances at the two wavelengths were measured by preparing a series of R-CQDs solutions with varied concentrations. The CF of R-CQDs is the slope of the curve between A_{280} and A_{350} (Figure S11).

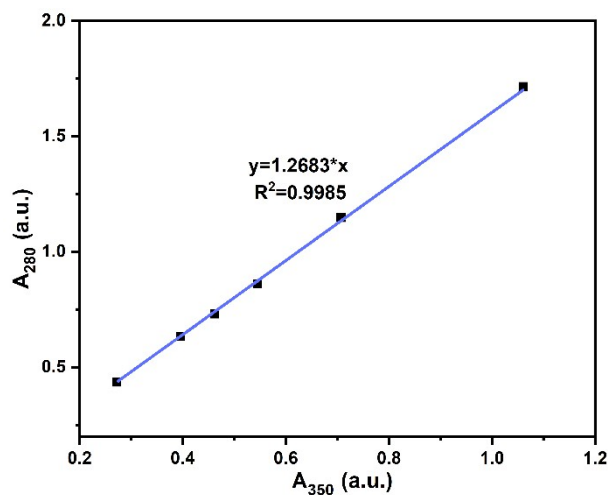


Figure S11. The relationship between the absorbance of R-CQDs at 280 nm and 350 nm.

16. Fluorescence intensity of the labeled BSA versus the reaction time

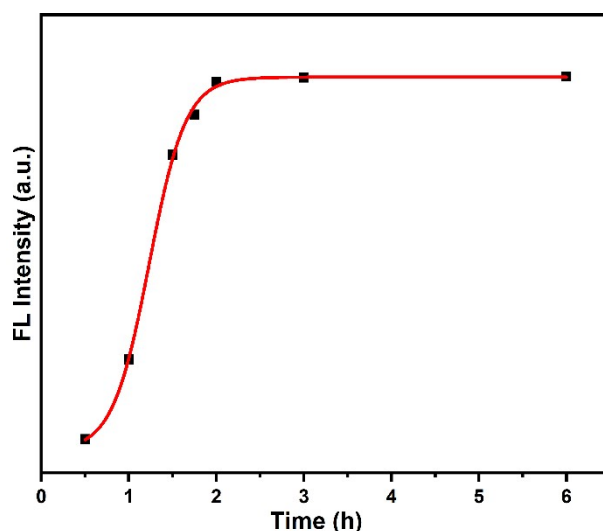


Figure S12. The curve between fluorescence intensity of labeled BSA ($\lambda_{\text{ex}}=550$ nm, $\lambda_{\text{em}}=615$ nm) and the labeling time (t).

17. Labeling of human serum albumin (HSA) by R-CQDs

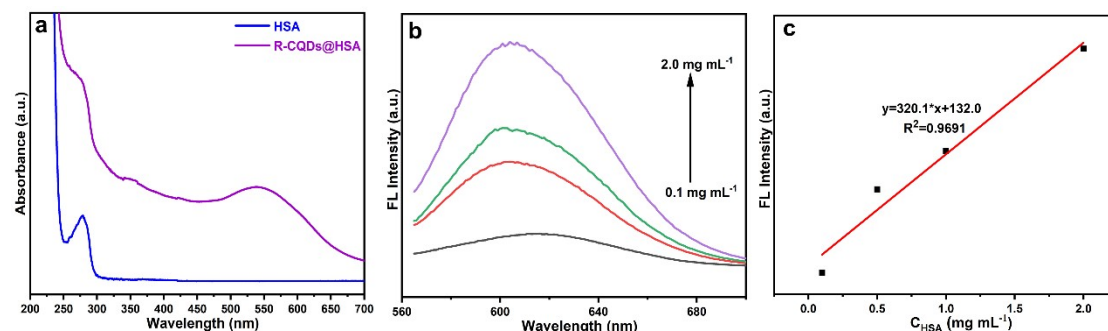


Figure S13. (a) UV-vis absorption spectra of HSA and R-CQDs@HSA. (b) The fluorescence spectra of HSA with varied concentrations labeled by 1.0 mg mL⁻¹ of R-CQDs. (c) The relationship between the fluorescence intensity and the HSA concentration.

It is shown from Figure S13 that HSA can also be efficiently labeled by R-CQDs and the fluorescence intensity also displays a good linearity versus the concentration of HSA. This work validates that the prepared R-CQDs is a novel and promising probe for labeling protein.

18. Influence of light on labeling efficiency

Figure S14 shows the labeling efficiency (LE) under daylight, dark and UV irradiation at 365 nm, respectively. It indicates that both LE and fluorescence intensity

of the R-CQDs@BSA are not influenced by light.

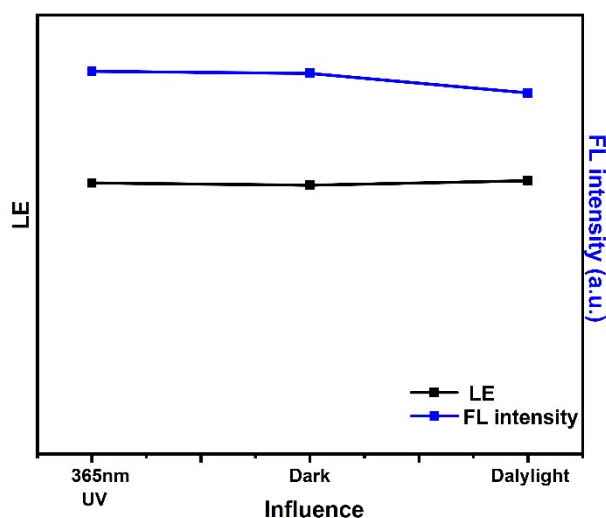


Figure S14. The influence of light on both the labeling efficiency and the fluorescence intensity of R-CQDs@BSA.

References:

1. B. I. Kurganov, A. V. Lobanov, I. A. Borisov, A. N. Reshetilov, Criterion for Hill equation validity for description of biosensor calibration curves, *Anal. Chim. Acta*, 2001, 427, 11–19.
2. P. del Pino, B. Pelaz, Q. Zhang, P. Maffre, G. U. Nienhaus, W. J. Parak, Protein corona formation around nanoparticles – from the past to the future, *Mater. Horiz.*, 2014, 1, 301–313.
3. S. H. Qu, F. Y. Sun, Z. H. Qiao, J. M. Li, L. Shang, In Situ Investigation on the Protein Corona Formation of Quantum Dots by Using Fluorescence Resonance Energy Transfer, *Small*, 2020, 16, 1907633.
4. R. G. Machicote, M. E. Pacheco, L. Bruzzone, Binding of several benzodiazepines to bovine serum albumin: Fluorescence study, *Spectrochim. Acta A Mol. Biomol. Spectrosc.*, 2010, 77, 466–472.
5. E. Lissi, C. Calderón, A. Campos, Evaluation of the number of binding sites in proteins from their intrinsic fluorescence: limitations and pitfalls, *Photochem. Photobiol.*, 2013, 89, 1413–1416.
6. N. A. Farid, N. F. Youssef, H. E. Abdellatef, Y. A. Sharaf, Spectrofluorimetric methods for the determination of mirabegron by quenching tyrosine and L-tryptophan fluorophores: Recognition of quenching mechanism by stern volmer relationship, evaluation of binding constants and binding sites, *Spectrochim. Acta A Mol. Biomol. Spectrosc.*, 2023, 293, 122473.